LAWRENCE
LIVERMORE
NATIONAL
LABORATORY

UCRL-JRNL-207241

Picosecond 14.7 nm interferometry of high intensity laser-produced plasmas

J. Dunn, J. Filevich, R. F. Smith, S. J. Moon, J. J. Rocca, R. Keenan, J. Nilsen, V. N. Shlyaptsev, J. R. Hunter, A. Ng, M. C. Marconi

October 15, 2004

Laser and Particle Beams

Picosecond 14.7 nm Interferometry of High Intensity Laser-Produced Plasmas

James Dunn[1], Jorge Filevich[2], Raymond F. Smith[1], Stephen J. Moon[1], Jorge J. Rocca[2], Roisin Keenan[1], Joseph Nilsen[1], Vyacheslav N. Shlyaptsev[3], James R. Hunter[1], Andrew Ng[1, 4], and Mario C. Marconi[2,5]

[1]Lawrence Livermore National Laboratory Livermore, CA 94551, USA
[2] NSF ERC for Extreme Ultraviolet Science and Technology and Dept. of Electrical and Computer Engineering, Colorado State University, Fort Collins, CO 80523, USA
[3]Department of Applied Science, University of California Davis-Livermore, Livermore, CA 94551, USA
[4]University of British Columbia, Vancouver
[5]Dept. of Physics, University of Buenos Aires, Argentina

Submitted to Laser and Particle Beams

Proceedings of 28th European Conference on Laser Interaction with Matter (ECLIM), Rome, Italy, 5 – 10 September, 2004

Corresponding author:

James Dunn
Lawrence Livermore National Laboratory
L-251, P.O. Box 808
Livermore, CA 94551
USA

Tel: + 925 423-1557
e-mail: dunn6 @llnl.gov

17 Pages
5 Figures

Abstract:

We have developed a compact, 14.7 nm, sub-5 ps x-ray laser source at LLNL together with a Mach-Zehnder type Diffraction Grating Interferometer built at Colorado State University for probing dense, high intensity laser-produced plasmas. The short wavelength and pulse length of the probe reduces refraction and absorption effects within the plasma and minimizes plasma motion blurring. This unique diagnostic capability gives precise 2-D density profile snapshots and is generating new data for rapidly evolving laser-heated plasmas. A review of the results from dense, mm-scale line focus plasma experiments will be described with detailed comparisons to hydrodynamic simulations.

Keywords:

x-ray laser, interferometry, laser-produced plasmas, x-ray optics

1. INTRODUCTION

Interferometry using optical wavelength laser beams was established as a powerful technique to probe dense plasmas within a few years of the invention of the laser (Alpher and White, 1965). Further development of the technique including utilizing a shorter wavelength, 4ω harmonic at 266 nm wavelength, and short duration, 15 ps, for the probe beam, was important to determine the electron density profile steepening at high laser intensities for laser-produced plasmas (Attwood *et al.*, 1978). The short pulse duration was essential for probing close to the target surface to freeze plasma motion. This trend to produce shorter wavelength probes was extended mainly to allow access to large plasmas at high density with less deleterious effects of absorption and refraction that strongly limit the applicability of visible or UV probes. The first soft x-ray laser interferometry was demonstrated by Da Silva and co-workers using the Nova high power laser-generated 15.5 nm Ne-like Y laser with a multi-layer coated beamsplitter Mach-Zehnder interferometer (Da Silva *et al.*, 1995). Large 1-mm-scale plasmas were probed to an electron density as high as 2×10^{21} cm^{-3} to within 25 μm of the initial target surface.

Recently, Rocca and co-workers established the 46.9 nm Ne-like Ar capillary discharge x-ray laser as a tabletop interferometric tool using first Lloyd's mirror and secondly Mach-Zehnder diffraction grating instrumentation (Rocca *et al.*, 1999; Filevich *et al.*, 2000). Further benefits can be achieved by going to shorter wavelengths if this can be combined with short pulse duration. The transient gain x-ray lasers have been shown to operate with small tabletop lasers of less than 10 J pump energy. It is possible to produce Ni-like ion 4d – 4p transition, 14.7 nm wavelength x-ray lasers in the saturation regime with greater than 10 μJ output energy and at a high repetition rate of 1 shot/4 minutes (Dunn *et al.*, 2000). This is sufficient output for applying tabletop, picosecond x-ray laser interferometry to laser-produced plasmas (Smith *et al.*, 2002; Filevich *et al.*, 2004). At this wavelength the critical density n_{crit} is 5.1×10^{24} cm^{-3} and so allows the probe to access much higher density plasmas.

Further progress in expanding the technique to different plasmas together with a better understanding of the x-ray source characteristics are reported in this paper.

2. DESCRIPTION

Details of the techniques to generate this x-ray laser (XRL) source on the LLNL Compact Multipulse Terawatt (COMET) laser can be found elsewhere (Dunn *et al.*, 2000; Smith *et al.*, 2002). For these experiments the short pulse pumping conditions are optimized to give both strong output and a 5 ps x-ray layer pulse duration by using a 6.7 ps laser pumping pulse (Dunn *et al.*, 2003). The pulse duration of the x-ray laser probe takes a snapshot image of the plasma to be probed and determines the temporal resolution for the interferometry. The Mach-Zehnder type interferometer for the 14.7 nm, picosecond duration x-ray laser, uses diffraction gratings as beam-splitters to generate and recombine the two beams (Filevich *et al.*, 2000; Filevich *et al.*, 2004). The gratings diffracting the x-ray laser at grazing incidence angles use well-established technology, have high throughput and are robust. This makes the Diffraction Grating Interferometer (DGI) well matched to soft x-ray laser lines over a broad spectral range, including the Ni-like ion Pd 4d – 4p x-ray laser at 14.7 nm wavelength. The x-ray laser output is relay imaged to the plasma (to be probed) using two high reflectivity Mo:Si multilayer coated mirrors. A normal incidence spherical mirror and a 45° flat mirror controlled by a stepper motor are used to align the beam under vacuum to the instrument. This has two advantages: it maximizes the x-ray laser fluence at the plasma and minimizes the steering of the beam due to variations in the XRL deflection angle as it exits the plasma. One major difference between this work and earlier x-ray laser interferometry (Da Silva *et al.*, 1995) is that with the 100× lower output available here, a substantial fraction of the x-ray laser beam is used to probe the plasma. One consequence is that this produces more constraints to the degree of overlap of the beams and spatial coherence of the source for the experiments reported here.

The first Au-coated grating *G1*, with 900 l/mm groove spacing, splits the XRL into a 0^{th} order (plasma probe) arm and a 1^{st} order (reference) arm, Fig. 1. The grating blaze angle and geometry have been designed to give equal reflectivity of ~25% in each arm. The two orders are reflected by the long Au-coated mirrors *L1* and *L2* to overlap the arms onto the second grating *G2*. The plasma to be probed is placed in the 0^{th} order beam at the position between *G2* and *L1*. The spherical multilayer mirror *IM* with 25 cm focal length, after *G2*, images the plasma and relays the beam via the output Au-coated mirror *L3* to the back-thinned charge-coupled device (CCD) camera. The total throughput of the instrument before the imaging optic *IM* is ~12%.

A second ruling of 16 l/mm is machined vertically offset on *G1* and *G2* substrates so that the instrument can be pre-aligned with an 827 nm infra-red (IR) diode laser. The IR laser has an estimated coherence length of ~300μm which is similar to the ~ 400 μm 1/e half width longitudinal coherence recently measured for the x-ray laser using a 6.7 ps pumping pulse (Smith *et al.*, 2003). The IR laser is used to adjust the various optics to make the two arms equal in length and for generating interference fringes. High quality 14.7 nm soft x-ray interference fringes have been generated with visibility exceeding 0.8. The magnification of the imaging system is set to give high x-ray laser fluence on the detector, effective working area at the plasma as well as good spatial resolution. The soft x-ray laser beam at the target position is imaged onto a 1.33 × 1.33 cm^2 CCD with 1024 × 1024 pixels of 13 × 13 μm^2 dimension. Magnification of 22 times is routinely used which gives a field of view of the plasma of ~600 × 600 μm^2. The pixel-limited spatial resolution is 0.6 μm with the overall spatial resolution of the instrument determined to be 1 – 2 μm.

3. RESULTS

We report results from several laser-produced plasma experiments that demonstrate probing long plasma columns generated by line focus incident on a 0.1 cm long Al slab target heated by the 600 ps (FWHM), 1054 nm laser of COMET. A maximum energy of 3 J was

available to produce a short line focus of 12 μm (FWHM) × 0.31 cm long using a combination of a cylindrical lens f = 200 cm and an off-axis paraboloid f = 30 cm. This corresponds to an incident laser intensity of ~10^{13} W cm^{-2}. The target rotation angle was carefully adjusted to ensure that the interferometer probe was parallel to the surface. The beams that form the x-ray laser and the second plasma to be probed come from the same oscillator and are synchronized. A delay line on the plasma-forming beam was adjusted for the x-ray laser to probe the plasma at various times from Δt = -0.5 to +3.0 ns, where Δt = 0 refers to the peak of the heating pulse. The absolute timing of the heating and x-ray laser beams was better than 100 ps while the x-ray laser pulse duration was ~5 ps.

Figure 2(a) shows one of a sequence of x-ray interferograms of the 0.1 cm long Al target recorded at +0.86 ns after the peak of the laser heating pulse. The 0.1 cm dimension of the plasma column is out of the page in the direction of the x-ray laser probe. It should be noted that there is very strong lateral expansion of the plasma along the target, vertical axis in Fig. 2(a), that is present almost immediately after the start of the laser pulse. So in addition to the expected strong expansion perpendicular to the target surface there is a very strong sideways component. A second feature is the small on-axis dip close to the target surface that is also observed in earlier time interferograms. This feature has not been seen on previous experiments at our laboratory with a wider line focus. The ability of the x-ray laser interferometry to probe close to the target surface allows this feature to be clearly seen. Simulations with the LASNEX hydrodynamics code (Zimmerman and Kruer, 1975) indicate that this is formed early on during the rising edge of the laser pulse and may be a result of the small line focus creating hot plasma conditions in a very localized region close to the target surface. The extracted 2-D electron density profile from the interferogram is shown in Fig. 2(b) and for comparison the 2-D LASNEX hydrodynamic simulations at +0.8 ns, Fig. 2(c). The laser pulse shape and focal spot shape are used in the simulations in order to model the experimental conditions as closely as possible. The overall agreement is good with some small differences on the sides of the plasma. Figure 3 shows an on-axis lineout of the

experimental data and simulations with generally good agreement. The maximum electron density measured is 4×10^{20} cm^{-3} close to the target surface where the fringe visibility becomes difficult to observe in the last 10 μm. It should be noted that at times later than +1 ns there is a reversal of the fringe direction close to the target surface (Filevich *et al.*, 2004b; Nilsen and Scofield, 2004). This is understood to be the contribution from the presence of low ionization stage bound electrons that for aluminum plasmas change the sign of the gradient of the index of refraction. This requires careful determination of the ionization of the plasma to interpret the fringe shifts (at late times) in extracting the electron density from the interferograms. It also makes the interferometry a very sensitive tool for probing low temperature plasmas.

A second run was carried out where a similar laser pulse was tightly focused at the center of the bottom of an Al groove of dimensions $100 \times 200 \times 1000$ μm^3 (H × D × L) machined by a diamond saw. This has the effect of confining the expansion of the plasma. The long axis of the line focus is aligned along the groove length. Figure 4, top image, shows the interferogram inside the groove before the laser pulse. The lower image, taken at +0.6 ns after the peak of the pulse, already shows a number of processes occurring. The plasma has expanded and hit the groove walls where there is now local heating in the corners. Plasma jets stream out from the corners and collide in the center of the groove. At later times low density material comes from the walls and a plasma jet streams out of the groove. At ~1 ns, the electron density is determined to be $1.2 \times 10^{21} cm^{-3}$ in the groove corners which is higher than the critical density of the laser heating beam. It should be possible to measure significantly higher electron densities with this technique by heating more target mass using higher energy beams focused to high intensity.

We have recently performed experiments to study long laser pulses incident in a tight focal spot on small lollipop targets to complement the lower intensity line focus plasma column experiments. Figure 5 shows two 14.7 nm soft x-ray interferograms of a 50 μm diameter lollipop target irradiated with a 20 J, 5 ns, 1064 nm flat top pulse generated by the

JANUS laser. This beam is focused to 20 μm (FWHM) diameter spot that corresponds to an intensity of 10^{15} W cm^{-2} on target. The target is constructed by etching a Si wafer 50 μm thick then coating on both sides with 7 μm parylene-C. The interferogram before the laser pulse is shown in Fig. 5(a). As in the previous examples the target is viewed from the side. Figure 5(b) at +4.8 ns, very close to the end of the laser pulse, shows the laser beam is incident from the right with strong plasma self-emission clearly visible on that side. The fringe shifts on the backside (left) of the target indicate plasma formation. The interferometer has been setup so that the plasma will induce fringe shifts towards the left. The lateral plasma expansion on the back surface is slightly larger than 100 μm with some indication that the target has disintegrated at the top. It is interesting to note that the plasma appears on the backside at fairly early times in the pulse and is expected to be mainly produced by plasma from the front surface streaming round the target rather than back surface release from laser-induced shock. While it would require Abel inversion to de-convolve the electron density profile, an estimate of the electron density can be deduced from the fringe shifts and plasma size. We estimate that the electron density is in excess of 5×10^{21} cm^{-3} for Fig. 3 (b) but a full analysis is required with a more symmetrical 2-D fringe pattern for more precise density measurements.

4. CONCLUSIONS

Picosecond x-ray laser interferometry at 14.7 nm of laser-produced plasmas has been successfully demonstrated using a Mach-Zehnder Diffraction Grating Interferometer. The combination of short wavelength and short pulse duration of the source and the high throughput of the instrument presents a unique diagnostic capability to study large, hot, dense plasmas. This technique can be applied to different target plasma geometries and has the potential to benchmark 2-D hydrodynamic simulations codes under a wide range of conditions. In addition to extracting 2-D density information from the interferograms, the technique can also quantify the degree of plasma ionization in low temperature aluminum plasmas. Plasmas created with laser pulses over 100 J energy and intensities up to 10^{15} W cm^{-2} have been studied and soft x-ray

interferograms have been recorded with ~1 μm spatial resolution close to the target surface. It is particularly important to note that the source, technique and instrumentation can be scaled to shorter wavelengths and can be applied to large plasmas generated on the National Ignition Facility and other large-scale, very dense plasmas. Further data analysis and simulations are in progress and will be reported shortly.

Work performed under the auspices of the US Department of Energy by the University of California Lawrence Livermore National Laboratory under Contract No. W-7405-Eng-48, through the Institute for Laser Science and Applications and by the National Nuclear Security Administration under the Stewardship Science Alliance Program through the US Department of Energy grant No. DOE-FG03-02NA00062.

REFERENCES

Alpher, R.A. and White, D.R. (1965). Optical Interferometry. In *Plasma Diagnostics Techniques*, (Huddlestone, R.H. and Leonard, S. L., Eds.) pp. 431 – 476. New York: Academic Press.

Attwood, D. T., Sweeney, D. G., Auerbach, J. M. and Lee, P. H. Y. (1978). Phys. Rev. Lett. **40**, 184-187.

Da Silva, L. B. Barbee, Jr., T. W., Cauble, R., Celliers, P., Ciarlo, D., Libby, S., London, R. A., Matthews, D., Mrowka, S., Moreno, J. C., Ress, D., Trebes, J. E., Wan, A. S. and Weber, F. (1995). Phys. Rev. Lett. **74**, 3991-3994.

Dunn, J., Li, Y., Osterheld, A. L., Nilsen, J., Hunter, J. R. and Shlyaptsev, V. N. (2000). Phys. Rev. Lett. **84**, 4834-4837.

Dunn, J., Smith, R.F., Shepherd, R., Booth, R., Nilsen, J., Hunter, J.R. and Shlyaptsev, V.N. (2003). *Soft X-ray Lasers and Applications V*. (Fill, E.E. and Suckewer, S., Eds.) SPIE Int. Soc. Opt. Eng. Proc, vol. **5197**, 51-59.

Filevich, J., Kanizay, K., Marconi, M. C., Chilla, J. L. A. and Rocca, J. J. (2000). Opt. Lett. **25**, 356 – 357.

Filevich, J., Rocca, J.J., Marconi, M. C., Smith, R. F., Dunn, J., Keenan, R., Hunter, J.R., Moon, S. J., Nilsen, J., Ng, A. and Shlyaptsev, V.N. (2004). Appl. Opt. **49**, 3938- 3946.

Filevich, J., Rocca, J.J., Marconi, M. C., Moon, S. J., Nilsen, J., Scofield, J.H., Dunn, J., Smith, R.F., Keenan, R., Hunter, J.R., and Shlyaptsev, V.N. (2004). "Observation of a multiply ionized plasma with index of refraction greater than one", submitted to Phys. Rev. Lett..

Nilsen, J., and Scofield, J.H. (2004). "Plasmas with an index of refraction greater than 1", Opt. Lett. **29**(22), in press.

Rocca, J.J., Moreno, C. H., Marconi, M. C. and Kanizay, K. (1999). Opt. Lett. **24**, 420–422.

Smith, R.F., Dunn, J., Nilsen, J., Shlyaptsev, V.N., Moon, S., Filevich, J., Rocca, J.J., Marconi, M.C., Hunter, J.R. and Barbee, Jr., T.W. (2002). Phys. Rev. Lett. **89**, 065004.

Smith, R.F., Dunn, J., Hunter, J.R., Nilsen, J., Hubert, S., Jacquemot, S., Remond, C., Marmoret, R., Fajardo, M., Zeitoun, P., Vanbostal, L., Lewis, C.L.S., Ravet, M.-F. and Delmotte, F. (2003). Opt. Lett. **28**, 2261–2263.

Zimmerman, G. B. and Kruer, W. L. (1975). Comments Plasma Phys. Controlled Fusion **2**, 51.

Figure Captions

Figure 1 Experimental setup showing soft x-ray Diffraction Grating Interferometer. X-ray laser enters and exits from right. CCD camera not shown is positioned approximately 5 meters from instrument.

Figure 2 (a) Soft x-ray interferogram of 1 mm long Al target recorded at +0.86 ns after the peak of the laser heating pulse. Initial focal spot is 12 μm (FWHM) and laser intensity is ~10^{13} W cm^{-2}. (b) Extracted 2-D electron density profile from interferogram. Electron density contour at 10^{20} cm^{-3} is indicated with the next two contours towards surface are 2×10^{20} and 3×10^{20} cm^{-3} while the next two contours away from the target surface are 9×10^{19} and 8×10^{19} cm^{-3}, respectively. (c) 2-D LASNEX simulations at +0.8 ns for the same laser plasma conditions.

Figure 3 On-axis electron density lineout from Fig. 2 showing experimental data points (diamonds) and 2-D LASNEX simulations (solid line).

Figure 4 Groove target $100 \times 200 \times 1000$ μm^3 (H × D × L) viewed along the long axis. Laser pulse incident from right. Top image shows interferogram before the laser pulse. Lower image is recorded at 0.6 ns after the peak of the laser pulse for a line focus plasma of 12 μm (FWHM) width × 0.31 cm at a laser intensity of ~10^{13} W cm^{-2}.

Figure 5 50 μm diameter lollipop target consisting of 50 μm thick Si coated with 7 μm parylene–C on each side viewed from the edge. (a) Interferogram of target before laser pulse. (b) Interferogram recorded at +4.8 ns after the start of the pulse. Laser pulse incident from right.

Fig. 1 DunnjXRL

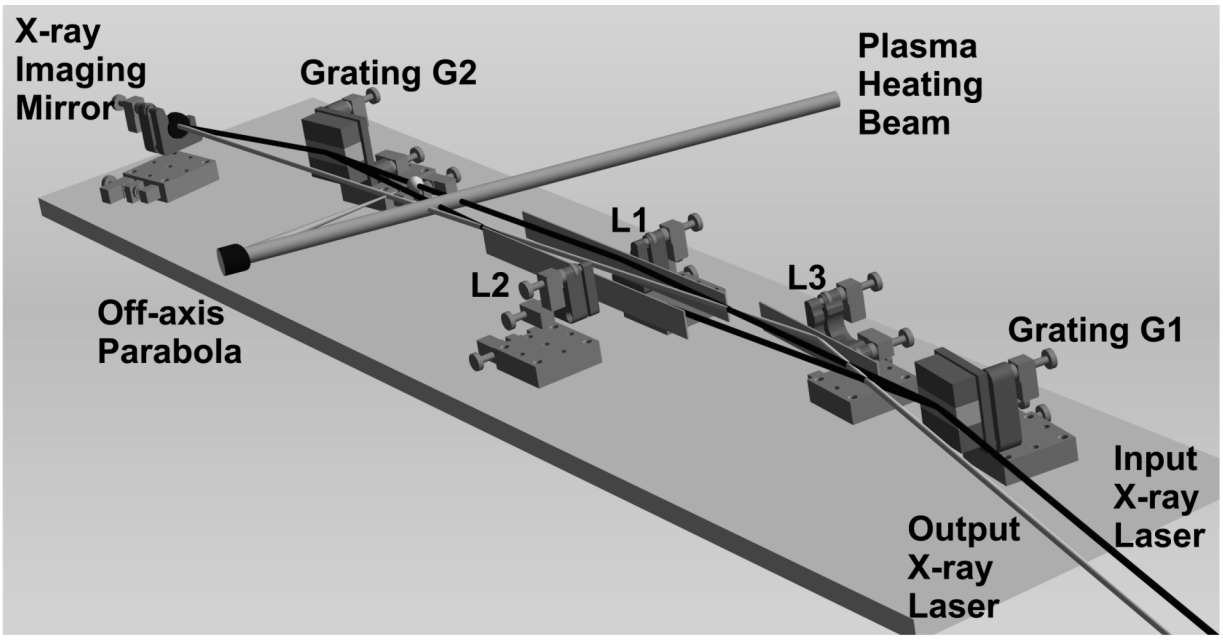

Fig. 2 DunnjXRL

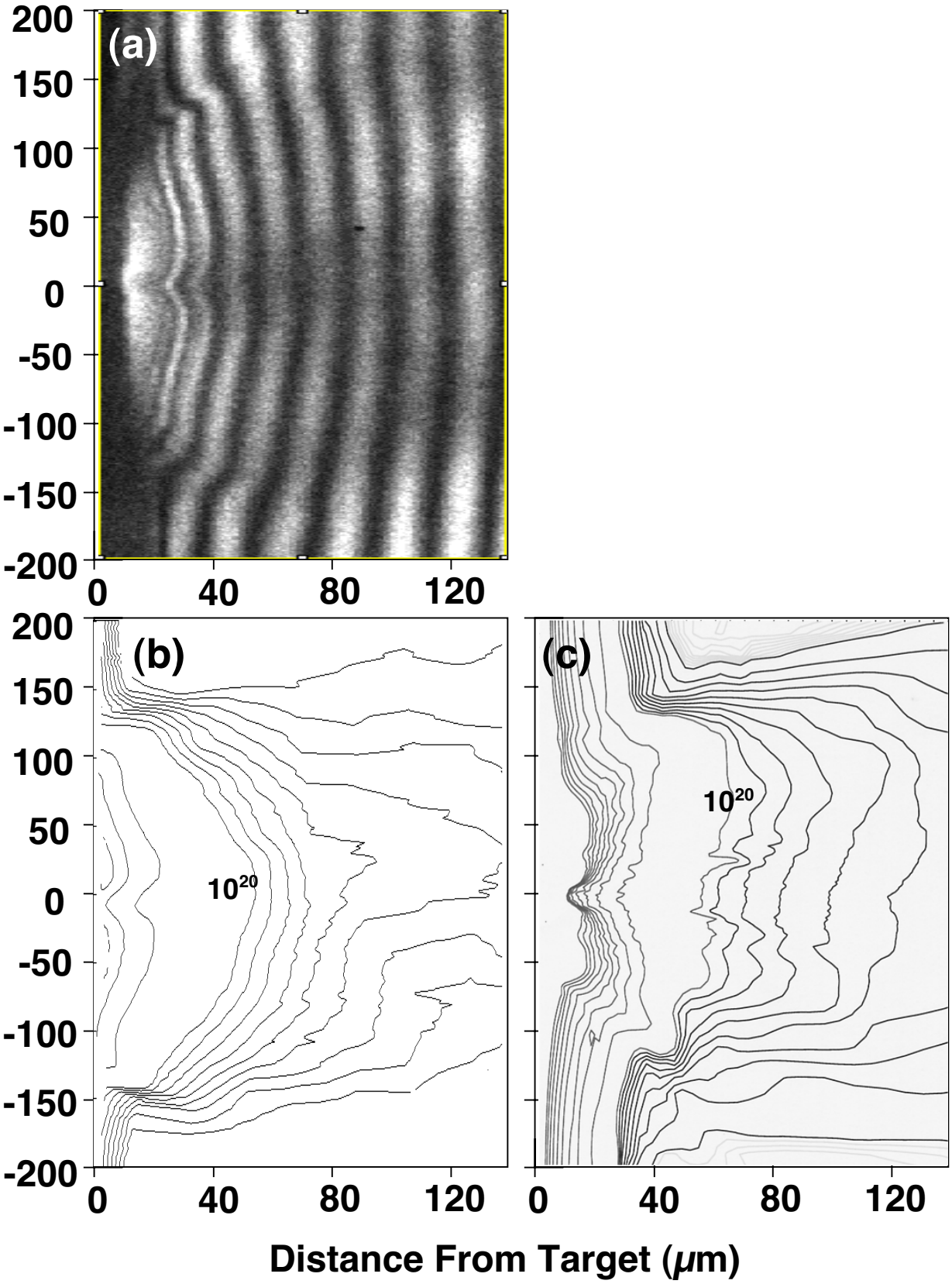

Fig. 3 DunnjXRL

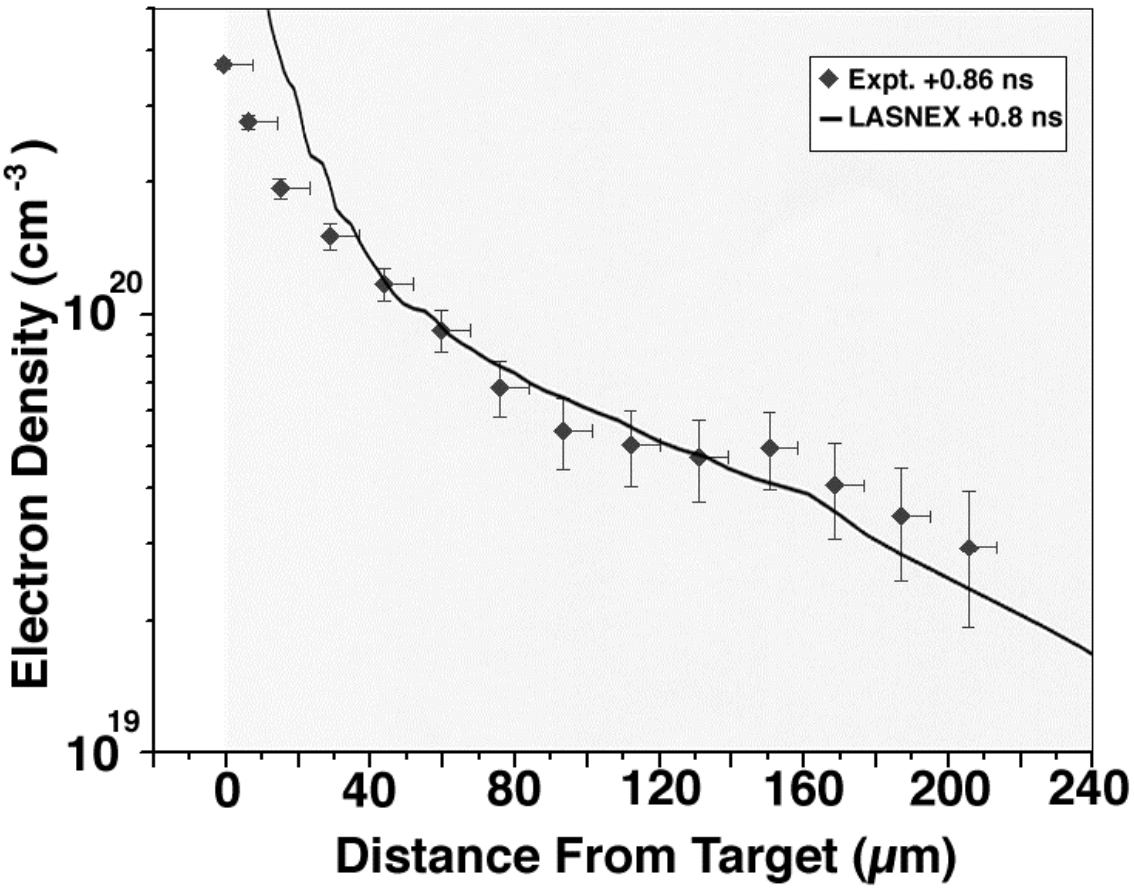

Fig. 4 DunnjXRL

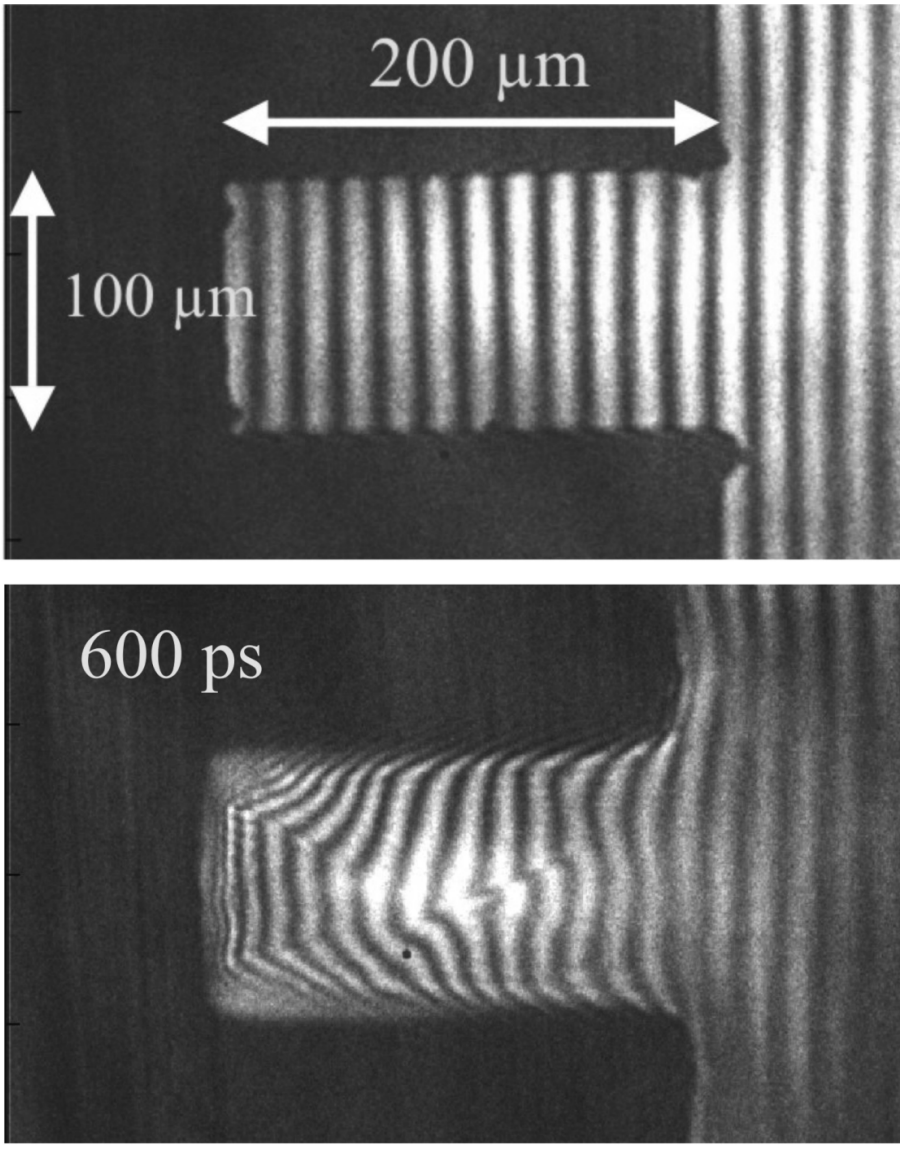

Fig. 5 DunnjXRL